Available online at www.sciencedirect.com
ScienceDirect
Ceramics International 34 (2008) 497–503
CERAMICS INTERNATIONAL
www.elsevier.com/locate/ceramint

Structure, magnetic and electrical transport properties of the perovskites $Sm_{1-x}Ca_xFe_{1-x}Mn_xO_3$

Guoyan Huo *, Dayong Song, Qing Yang, Fuying Dong

School of Chemistry and Environmental Science, Hebei University, Baoding 071002, PR China

Received 15 September 2006; received in revised form 28 September 2006; accepted 24 November 2006
Available online 28 December 2006

Abstract

The structure of series $Sm_{1-x}Ca_xFe_{1-x}Mn_xO_3$ ($0.0 \leq x \leq 1.0$) compounds was investigated. The lattice parameters increase with coupled substitution Sm^{3+} by Ca^{2+} and Mn^{4+} for Fe^{3+}. The variation of parameter, *c*, is larger than that of *a* and *b*, respectivly. The detailed analysis of magnetic properties of series $Sm_{1-x}Ca_xFe_{1-x}Mn_xO_3$ ($0.1 \leq x \leq 0.9$) shows that local magnetic interaction between Fe^{3+} and Fe^{3+} and Mn^{4+} and Mn^{4+} at below magnetic transition temperature is antiferromagnetic. Above magnetic transition temperature the presence of large magnetic cluster is proposed and the sizes of magnetic clusters decrease with Mn^{4+}. The electrical transport behaviors related with small polaron hopping and variable range hopping models.

Keywords: C. Magnetic properties; Structure; Electrical transport behavior; Serial compounds

1. Introduction

A lot of work has been devoted to hole doped manganites $Ln_{1-x}A_xMnO_3$ with $x < 0.5$ since the discovery of colossal magnetoresistance (CMR) in these materials [1–5]. For those Mn (III)-rich manganites, it was shown that there exists a critical average size of the interpolated cation below which the CMR effect does not appear [6]. This is, for instance, the case of the samarium–calcium compounds that are semiconductors in the absence of magnetic field and do not exhibit any CMR effect up to 7 T whatever *x*, ranging from 0 to 0.50, due to the small average size of A-site cations (1.132 Å $< \langle r \rangle <$ 1.156 Å) and to the small A-site cationic size mismatch σ^2 [7]. In contrast, the Mn (IV)-rich manganites were investigated extensively until now [8–10]. Based on the study of the oxides $Ca_{1-x}Bi_xMnO_3$ [11] and $Ca_{1-x}Eu_xMnO_3$ [12] metal-insulator transitions and consequently, CMR properties were shown recently in the oxides $Ca_{1-x}Ln_xMnO_3$ with $x = 0.13$–0.15 [13,14]. The striking feature of these electron-doped manganites is that the CMR effect appears for a very small size of the interpolated cation contrary to the hole-doped manganite that require high $\langle r \rangle$ values for the appearance of the CMR effect. Moreover, the homogeneity range where the CMR effect appears is very narrow compared with the hole-doped manganites, *x* ranging typically from 0.12 to 0.15. In fact, it was shown with the study of the oxides $Ca_{1-x}Th_x MnO_3$ and $Ca_{1-x}Ce_x MnO_3$ [14], that in this case, it is the electron density that plays a critical role for the appearance of the CMR properties.

The research work reported by Takeuchi et al. [15] suggests that Fe substitution for Mn dilutes the double exchange (DE) mechanism and shows typical spin glass and insulating behaviors. The results of several authors studied the $Ln_{1-x}A_xMn_{1-y}Fe_yO_3$ Fe-doped manganites with $y \leq x$ indicate that Fe and Mn host lattice is antiferromagnetic interaction [16–18].

To our knowledge, there is little data, which are available on coupled A–B-site substitutions in ABO_3 [19,20]. On the basis of previously published experimental data, we may expect that a coupled substitution involving Sm and Fe would improve the properties of $CaMnO_3$. So if Sm is doped at Ca-site and Fe doped at Mn-site, useful information for understanding could be obtained.

The purpose of the present study is to clarify the magnetic properties and transport mechanism in mixture of manganites $Sm_{1-x}Ca_xFe_{1-x}Mn_xO_3$ and to show how the properties change with the replacement of Sm by Ca and Fe by Mn.

* Corresponding author. Tel.: +86 312 5079359; fax: +86 312 5079525.
E-mail address: guoyanhuo@yahoo.com.cn (G. Huo).

0272-8842/$34.00 © 2007 Published by Elsevier Ltd and Techna Group S.r.l.
doi:10.1016/j.ceramint.2006.11.010

2. Experimental

Polycrystalline samples of $Sm_{1-x}Ca_xFe_{1-x}Mn_xO_3$ ($0.0 \leq x \leq 1.0$) were prepared by standard solid-state reaction from stoichiometric amounts of Sm_2O_3, $CaCO_3$, Fe_2O_3 and MnO_2, which the purities of them are, at least, 99.9%. A purity of 99.99% Sm_2O_3 powders was dried for 5 h at 800 °C before used. The mixtures were ground by hand in a mortar agate for at least 40 min and pressed into pellets, then preheating the pellets for 8 h at 800 °C. Following the mixtures was ground extensively once again. Then the powders were pressed into pellets and annealed at 1100 °C in air for 16 h with intermediated grindings and finally cooled the samples down to 500 °C at 1 °C/min, then cooled to room temperature in furnace.

Phase analysis and characterization were carried out by X-ray diffraction (XRD) using Cu Kα radiation with a graphite monochromator on Rigaku model D/max-2400 X-ray diffractometer at room temperature.

Temperature dependence of magnetization curve was measured by a vibrating sample magnetometer (VSM) in a field of 0.5 T over the temperature range 80–300 K. Electrical resistances were determined by the standard four-probe DC method in the range 300–500K.

3. Results and discussion

3.1. Crystal structure

The products of synthesis by standard solid state technique yielded single-phase materials, which were confirmed by powder XRD. The XRD patterns of all samples can be indexed on basis of the $CaMnO_3$ type with orthorhombically distorted perovskite structure (space group *Pbnm*). This type of structure is common for rare earth perovskite-type oxides. Each unit cell consists of four ABO_3 units, and has the approximate dimensions $\sqrt{2}a_p \times \sqrt{2}a_p \times 2a_p$, where a_p is the lattice parameter of the ideal cubic unit cell. On regular sites, a Ca^{2+} cation on a Sm^{3+} lattice position and a Mn^{4+} cation on a Fe^{3+} position in the perovskite lattice. The lattice parameters of the orthorhombic cell determined by XRD are shown in Fig. 1 and Table 1. It can be seen from Fig. 1 that the orthorhombic lattice parameters decrease with Ca^{2+} and Mn^{4+} content in $Sm_{1-x}Ca_xFe_{1-x}Mn_xO_3$ and that the change of lattice parameters, a and b, are relatively small compared to that of c, this is due to the tilting scheme of BO_6 octahedral in *Pbnm* perovskite, of the type $a^-a^-c^+$ in Glazer's nomenclature [21], in which the distortion driven by the increase of average A size and by the reduction of average B size leaves c changed quickly. The variation of cell parameter, a, is relatively big compared with that of b in the range from $x = 0.0$ to 0.5, while the change of this parameter is smaller than that of b in the range from $x = 0.5$ to 1.0, indicating that the substitution of Ca^{2+} for Sm^{3+} and Mn^{4+} for Fe^{3+} is not random. Whilst, the variance of lattice parameters confirm that the compounds form solid solutions but not two compounds simply mixed. The observed unit cell volume decreases with the coupled substitution of Sm by Ca with that of the Fe by Mn (see Fig. 2). It is worth noting that, in all cases, $c/\sqrt{2}$ lies between a and b ($b < c/\sqrt{2} < a$, see Table 1). This is characteristic of the so-called O structure and constitutes the usual situation in perovskites where the primary the distorting effect is steric factor. The spontaneous orthorhombic strain, defined as $s = 2(a - b)/(a + b)$, is included in Table 2. s progressively decreases from $x = 0.0$ to 0.5 following increases from $x = 0.5$ to 1.0 perovskites. The reason for the decrease of this parameter from $x = 0.0$ to 0.5 is that on A site the substitution of big radius Ca^{2+} for small radius Sm^{3+} and on B site the replacement of big radius Fe^{3+} by small radius Mn^{4+}, the reduction out of phase tilting caused by distortions of the O–B(Fe)–O angles of the octahedral for fitting the size of A average size plays a important role [22,23]. The reason for

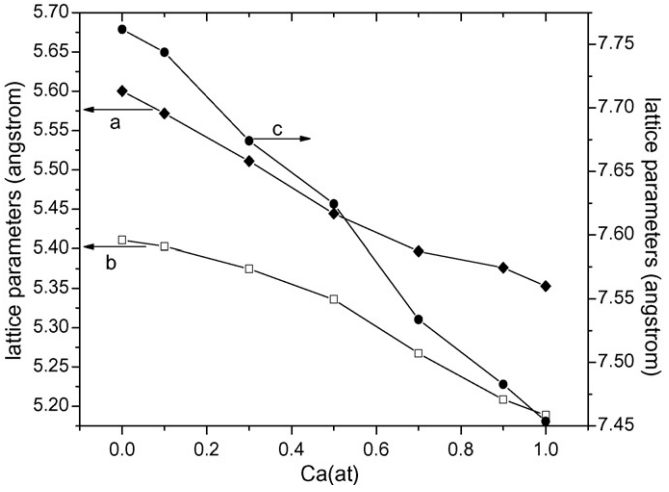

Fig. 1. Lattice parameters (a, b, c) of $Sm_{1-x}Ca_xFe_{1-x}Mn_xO_3$ ($0.0 \leq x \leq 1.0$) as a function of Sm content.

Table 1
Lattice parameters, relationship of a, b, c, and type of orthorhombic structure of the system $Sm_{1-x}Ca_xFe_{1-x}Mn_xO_3$ ($0.0 \leq x \leq 1.0$)

x	a	b	c	$c/\sqrt{2}$	a, b, $c/\sqrt{2}$ relation	Structure type
0.0	5.6004	5.4108	7.7618	5.4884	$b < c/\sqrt{2} < a$	O-type
0.1	5.5716	5.4030	7.7438	5.4757	$b < c/\sqrt{2} < a$	O-type
0.3	5.5112	5.3746	7.6740	5.4263	$b < c/\sqrt{2} < a$	O-type
0.5	5.4444	5.3358	7.6244	5.3913	$b < c/\sqrt{2} < a$	O-type
0.7	5.3966	5.2672	7.5338	5.3727	$b < c/\sqrt{2} < a$	O-type
0.9	5.3761	5.2085	7.4828	5.2911	$b < c/\sqrt{2} < a$	O-type
1.0	5.3592	5.1889	7.4536	5.2707	$b < c/\sqrt{2} < a$	O-type

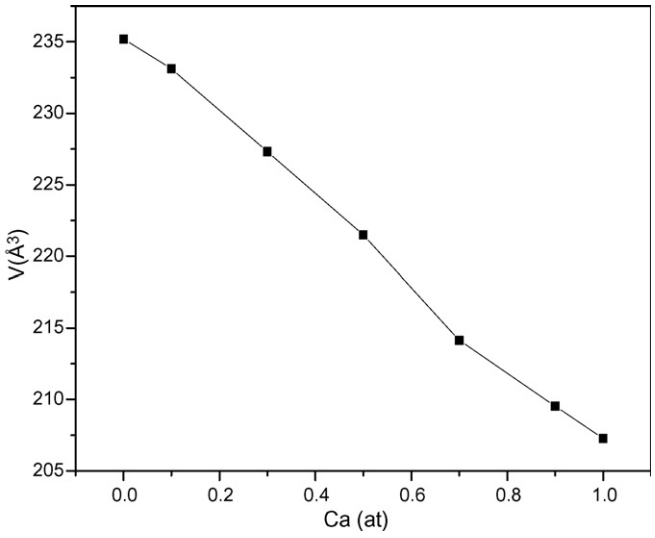

Fig. 2. Unit cell volume of $Sm_{1-x}Ca_xFe_{1-x}Mn_xO_3$ ($0.0 \leq x \leq 1.0$) as a function of Sm content.

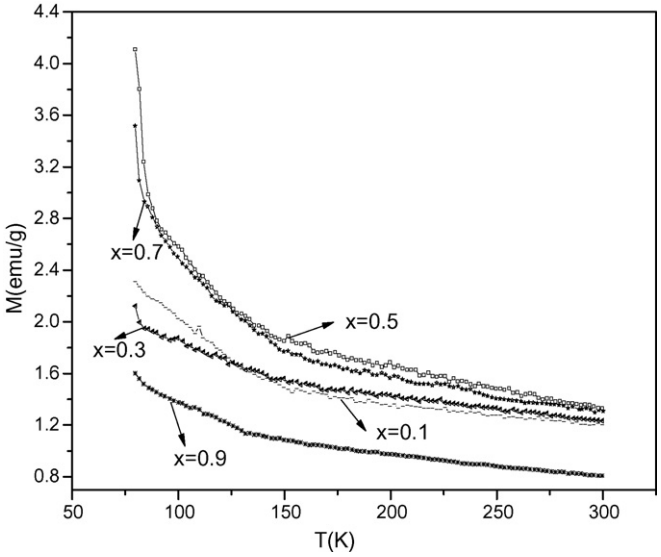

Fig. 3. The temperature dependence of magnetization (M) of $Sm_{1-x}Ca_xFe_{1-x}Mn_xO_3$ samples measured under $H = 0.5$ T.

increase of s from $x = 0.5$ to 1.0 is that A site average size increases with Ca^{2+} substituting for Sm^{3+} and B site average size decreases with replacing Fe^{3+} by Mn^{4+}, the octahedral tilting driven by out of phase increases for matching the reduction of A site average size. The values of the cell distortion factor d for $Sm_{1-x}Ca_xFe_{1-x}Mn_xO_3$ are also useful for estimating the departure from the ideal cubic cell:

$$d = \frac{[(a/\sqrt{2} - a_p)^2 + (b/\sqrt{2} - a_p)^2 + (c/2 - a_p)^2]}{3a_p} \times 10^4$$

where $a_p = (a/\sqrt{2} + b/\sqrt{2} + c/2)/3$ are also given in Table 2. This factor changes tendency similar to that of spontaneous orthorhombic strain s. It is worth mentioning that the variation of the a parameter is big compared to that of b with coupled substitution from $x = 0$ to 0.5, which coincides the spontaneous orthorhombic strain, s, and cell distortion factor, d, lowering from big value to small one and that the variation of the b parameter is big compared to that of a with coupled replacement from $x = 0.5$ to 1.0, which coincides the spontaneous orthorhombic strain, s, and cell distortion factor, d, increaseing from low value to high one. According to analysis mentioned above, the variance of lattice parameters with coupled substitution on A site and on B site is the results of changes of distorted BO_6 octahedra for matching A sizes.

3.2. Magnetic properties

Fig. 3 presents the temperature-dependent magnetization (M–T) of the $Sm_{1-x}Ca_xFe_{1-x}Mn_xO_3$ ($0.1 \leq x \leq 0.9$) system under a magnetic field of 0.5 T. It can be seen from Fig. 3 that the magnetic transition temperatures of the samples are below 80.0 K. The susceptibility presents the Curie–Weiss type behavior [$\chi = C/(T - \theta_{CW})$] for the temperatures above 80.0 K. Here, C and θ_{CW} are Curie constant and Curie–Weiss temperature, respectively. The values of θ_{CW} of all samples are negative (see Fig. 4 and Table 2), indicating that the local magnetization below magnetic transition temperatures are associated with the antiferromagnetic coupling. Curie–Weiss temperature is related to the strength of antiferromagnetic interaction. With the increase Ca^{2+} and Mn^{4+} contents from 0.1 to 0.5 the Curie–Weiss temperatures increase to high temperatures. This indicates that antiferromagnetic interactions sharply become weak. With increasing Ca^{2+} and Mn^{4+} content

Table 2
The unit cell volume, the tolerance factor (t) and spontaneous orthorhombic strain (s)

	x						
	0.0	0.1	0.3	0.5	0.7	0.9	1.0
V (Å^3)	235.203	233.114	227.308	221.490	214.148	209.529	207.272
t	0.9128	0.9215	0.9390	0.9570	0.9754	0.9943	1.0091
s	0.03444	0.03072	0.02510	0.02015	0.02427	0.03167	0.03229
d	7.7873	5.6348	4.1236	2.5789	3.7086	6.2560	6.4854
θ_{CW} (K)		−500	−463	−237	−274	−282	
$C_{obsd.}$ (K emu mol^{-1} G^{-1})		49.37	36.78	30.56	26.28	15.54	
$C_{calc.}$ (K emu mol^{-1} G^{-1})		4.20	3.69	3.17	2.65	2.13	
$C_{obsd.}/C_{calc.}$		11.8	10.0	9.6	9.9	7.3	

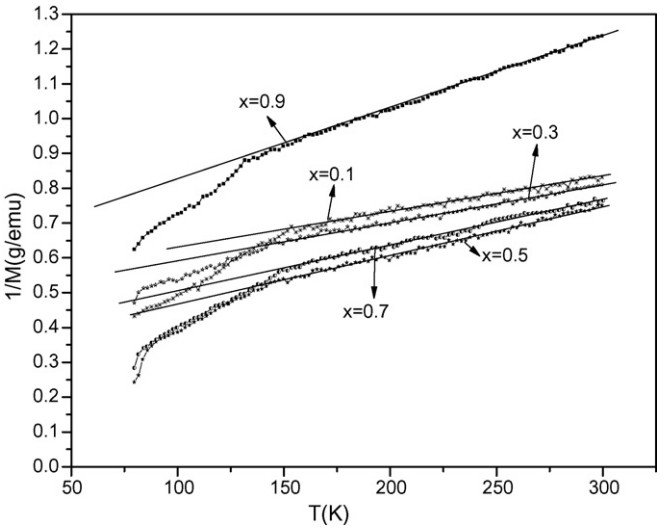

Fig. 4. The temperature dependence of reciprocal magnetization ($1/M$) for $Sm_{1-x}Ca_xFe_{1-x}Mn_xO_3$ samples, the solid lines are fits to the Curie–Weiss law.

from 0.5 to 0.9 the Curie–Weiss temperatures slightly decrease to low temperatures. From the variation of Curie–Weiss temperature with Ca^{2+} content (x) (see Table 2) it can be inferred that the double exchange interactions between neighboring Fe^{3+} or Mn^{3+} and Fe^{4+} or Mn^{4+} ions is relatively strong but short range interactions which are responsible for the formation of the ferromagnetic correlation as overlapping of $e_g^{\uparrow}$ for Fe^{3+} and $e_g^{\uparrow}$ for Mn^{4+} to produce little amount of Mn^{3+} and Fe^{4+} [24] and that the exchange interactions between Fe^{3+} or Mn^{4+} and Fe^{3+} or Mn^{4+} are strong and long range antiferromagnetic. Therefore, the antiferromagnetic interaction is strengthed in the Fe^{3+} dominant range or in the Mn^{4+} dominant range [24] and the Curie–Weiss temperature reduces to lower temperature. In other words, with Mn^{4+} substitution for Fe^{3+} up to Mn^{4+} content 0.5 Mn^{3+} concentration increases, resulting in Curie–Weiss temperature fast moves to high temperature, following with further increasing Mn^{4+} content from 0.5 to 0.9 Mn^{3+} concentration decreases, leading to Curie–Weiss temperature changes to slightly low temperature. The values of the deriving parameters θ and Curie constant from Fig. 4 and theoretical Curie constant values are listed in Table 2.

As shown in Table 2, the experimental Curie constant C takes the value between 15 and 50 emu K/mol G. Assuming that there is no coupling among the ions on Sm, Fe and Mn sites, the theoretical Curie constant can be expressed as $C = N_A(\mu_{eff})^2/3k_B$, here N_A is Avogadro number and μ_{eff} is the average effective magnetic moment for Sm, Fe and Mn sites. Considering that the effective magnetic moment is $3.87\mu_B$ for Mn^{4+} ($S = 3/2$), $5.92\mu_B$ for Fe^{3+} (HS, $S = 5/2$) $0.84\mu_B$ for Sm^{3+} ($S = 5/2$), the ideal value of Curie constant for $Sm_{1-x}Ca_xFe_{1-x}Mn_xO_3$ is estimated and listed in Table 2. It can be clearly seen from Table 2 that the experimental value of C is about 7–12 times larger than that theoretically predicated. This difference suggests the existence of the strong coupling among the Mn^{4+} and/or Fe^{3+} ions, which may be led to the formation of magnetic clusters. A simple estimate shows that to meet the gap between the calculated and observed Curie constants, magnetic clusters of 7–12 Mn^{4+} or/and Fe^{3+} ions have to be assumed. Comparison the experimental with ideal Curie constants in Table 2 it is suggested that the transition metal ionic numbers of each magnetic cluster decrease with Mn^{4+} and Ca^{2+} ions doped and that the ferrite oxides is easier to form magnetic cluster than that of manganite oxides. In fact, the presence of magnetic clusters in paramagnetic phase of manganite oxides was also reported by several groups [25–27]. For example, using the Curie–Weiss law, Kumar et al. [26] studied the susceptibility of polycrystalline $La_{0.7}Ca_{0.3}MnO_3$, and suggested the formation of magnetic clusters of two Mn ions in the temperature range $250\ K < T < 340\ K$ to account for a doubled Curie constant (compared with the ideal value). Similar results to ours, localized magnetic cluster with a size of 1.2 nm was reported by Teresa et al. [28] for $(La_{1-x}Y_x)_{0.67}Ca_{0.33}MnO_3$. The size of magnetic cluster in our results are larger than usual ones, this may be related to large applied magnetic field (0.5 T) in our experiment. Teresa et al. [28] have reported that size of magnetic clusters is related to magnetic field and increase magnetic clusters with magnetic field.

3.3. Electrical transport properties

As the resistivity of serial $Sm_{1-x}Ca_xFe_{1-x}Mn_xO_3$ ($0.0 \le x \le 0.9$) compounds is very high at room temperature and shows the insulating behavior, therefore, the electrical transport properties are studied in the range from 300 to 500 K. Fig. 5 presents the temperature-dependent resistivity ($\rho - T$) of the $Sm_{1-x}Ca_xFe_{1-x}Mn_xO_3$ ($0.0 \le x \le 0.9$) system from 300 to 500 K. Even room temperature the resistivity of $SmFeO_3$ sample is too large to determine, therefore, the resistivity of this specimen didn't include this investigate. It can be seen from Fig. 5 that the resistivity of the samples decreases with temperature and shows the insulator properties. One also notices that the resistivity reduces with coupled substitution of Ca^{2+} for Sm^{3+} and Mn^{4+} for Fe^{3+}. The reason is described as following. In perovskite oxides, the d electrons of the Mn and Fe ions are known to stay in the same spin state, due to the

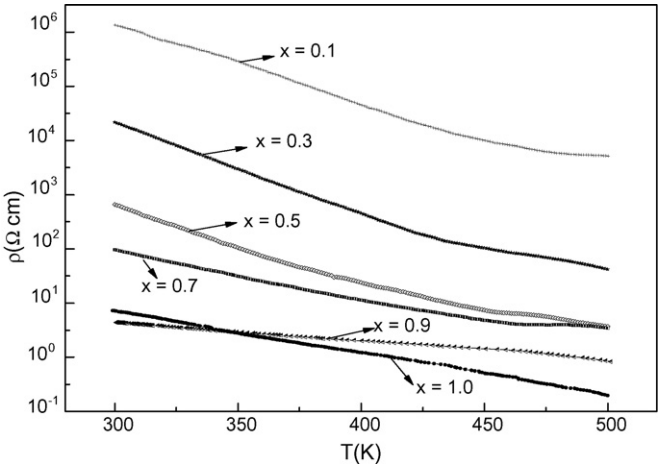

Fig. 5. The temperature-dependent resistivity ($\rho - T$) of the $Sm_{1-x}Ca_xFe_{1-x}Mn_xO_3$ ($0.0 \le x \le 0.9$) specimens.

strong Hund's coupling. The vacant state with opposite spin lies higher in energy due to exchange interactions. Both occupied and unoccupied spin states are further split into t_{2g} and e_g orbitals by the octahedral crystal field. Increasing energy, these states are $t_{2g\uparrow}$, $e_{g\uparrow}$, $t_{2g\downarrow}$ and $e_{g\downarrow}$. The electeonic configurations are $t_{2g\uparrow}^3 e_{g\uparrow}^2$ for Fe^{3+}, $t_{2g\uparrow}^3 e_{g\uparrow}^1$ for Fe^{4+}, and Mn^{3+} and $t_{2g\uparrow}^3$ for Mn^{4+}, respectively. In a solid, these states form bands. For these ions, the $t_{2g\uparrow}$ bands are fully occupied, the $t_{2g\downarrow}$ and $e_{g\downarrow}$ are empty, and $e_{g\uparrow}$ bands, which can accomodate a maxmium of two electrons per ion, play a crucial role. In a mixed system of Fe and Mn, the widths and energies of their $e_{g\uparrow}$ bands dictate the electron distribution of the Fe and Mn ions. Joonker [29] studied the conductivity of $La_{0.85}Ba_{0.15}Mn_{1-x}Fe_xO_3$ compound and showed that for $0 < x < 0.85$, Fe^{3+}, Mn^{3+} and Mn^{4+} are present, and for $0.85 < x < 1.00$, Fe^{3+}, Fe^{4+} and Mn^{4+} are present. The existence of Fe^{3+}, Mn^{3+} and Mn^{4+} in the range of $0 < x < 0.85$, indicates that the Fe $e_{g\uparrow}$ band is full and the Mn $e_{g\uparrow}$ band is less than half-filled. For $0.85 < x < 1.00$, the existence of Fe^{3+}, Fe^{4+} and Mn^{4+} means an empty Mn $e_{g\uparrow}$ band and a more than half-filled Fe $e_{g\uparrow}$ band. From this, it can be inferred that the bottom of the Mn $e_{g\uparrow}$ band should be at the same level as, or higher than, the top of the Fe $e_{g\uparrow}$ band. Therefore, the Fe $e_{g\uparrow}$ band remains completely filled as long as the Mn $e_{g\uparrow}$ band is partially filled. A similar conclusion has been reached by studying the structural and conduction properties of a closely related system of $La_{1-x}Ca_xFe_{1-x}Mn_xO_3$. They found that most Fe is present as Fe^{3+}, and at least 97% of the Mn exists as Mn^{4+} [30]. They proposed the presence of a small amount (less than 3%) of Mn^{3+} and Fe^{4+} to account for the conductivity behavior in their samples. This conclusion agrees with the band structure mentioned above, where the top of the Fe $e_{g\uparrow}$ band is nearly at the bottom of the Mn $e_{g\uparrow}$ band, except for a slight overlap (less than 3%) between the two, as shown in Fig. 6. Our system of $Sm_{1-x}Ca_xFe_{1-x}Mn_xO_3$ ($0.0 \le x \le 0.9$) is expected to have a similar band structure as that of $La_{1-x}Ca_xFe_{1-x}Mn_xO_3$. This energy diagram clearly shows that part $e_{g\uparrow}$ electrons of Fe^{3+} occupy part $e_{g\uparrow}$ orbitals of Mn^{4+} to produce a little amount of Fe^{4+} and Mn^{3+}. It is clear that electron hopping paths from Mn^{3+} to Mn^{4+} and/or Fe^{3+} to Fe^{4+} are permitted. With coupled substitution of Ca^{2+} for Sm^{3+} and Mn^{4+} for Fe^{3+} increasing the amount of Fe^{4+} and Mn^{3+} is augmented and resistivity of serial compounds is reduced untill to $x = 0.9$. As there is no Fe^{4+} in the $CaMnO_3$ compound and electron hopping from Fe^{3+} to Fe^{4+}, thereby, its resistivity is higher than that of $x = 0.9$ around room temperature. But the resistivity of this end member is not so high, this may attribute to a little amount of Mn^{3+} caused by shortage of oxygen.

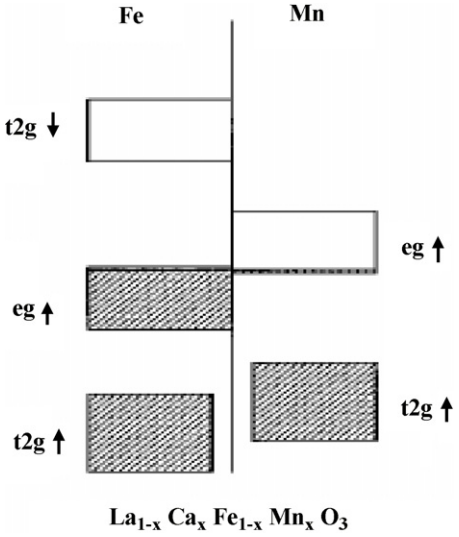

Fig. 6. Band structure of Fe and Mn in $La_{1-x}Ca_xFe_{1-x}Mn_xO_3$, where the bottom of the Mn $e_{g\uparrow}$ band lies slightly below the top of the Fe $e_{g\uparrow}$ band.

In order to get more insight into the transport processes, the electrical resistivity data were fitted to various model applied for materials including:

$$\rho = \rho_0 \exp\left(\frac{E_A}{kT}\right) \quad (1)$$

$$\rho = \rho_0 T \exp\left(\frac{E_A}{kT}\right) \quad (2)$$

$$\rho = \rho_0 T^{1/2} \exp\left(\frac{E_A}{kT}\right) \quad (3)$$

$$\rho = \rho_0 T^{3/2} \exp\left(\frac{E_A}{kT}\right) \quad (4)$$

$$\rho = \rho_0 \exp\left(\frac{T_0}{T}\right)^{1/4} \quad (5)$$

$$\rho = \rho_0 T \exp\left[\frac{E}{kT} + \left(\frac{T_0}{T}\right)^{1/4}\right] \quad (6)$$

where E is the energy difference between the initial and intermediate state and $k_b T_0 = 18\alpha^3/n(E_F)$; α is the inverse of localization length and $n(E_F)$ is electronic density of state at Fermi level. Above expressions are formula for thermal activation, adiabatic polaron, bipolaron, non-adiabatic polaron, variable range hopping and two steps transport of small polarons [31] models, respectively. Fig. 7 shows the electrical transport behaviors for $x = 0.1$ sample at high temperature and inset of

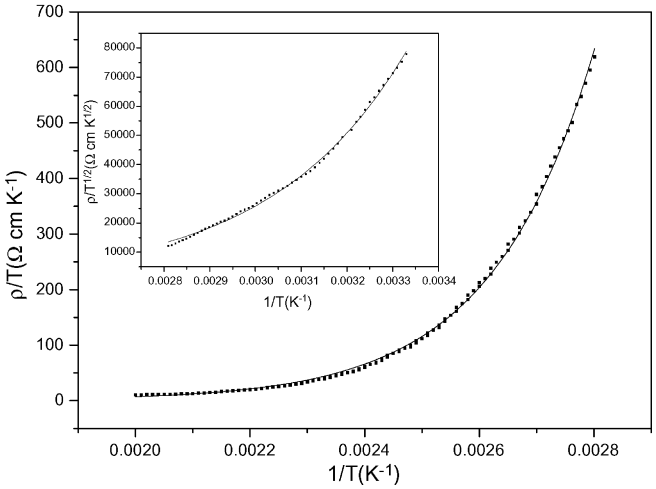

Fig. 7. Fitting curve based on $\rho = \rho_0 T \exp(E_A/kT)$, in set is fitting line based on $\rho = \rho_0 T^{1/2} \exp(E_A/kT)$.

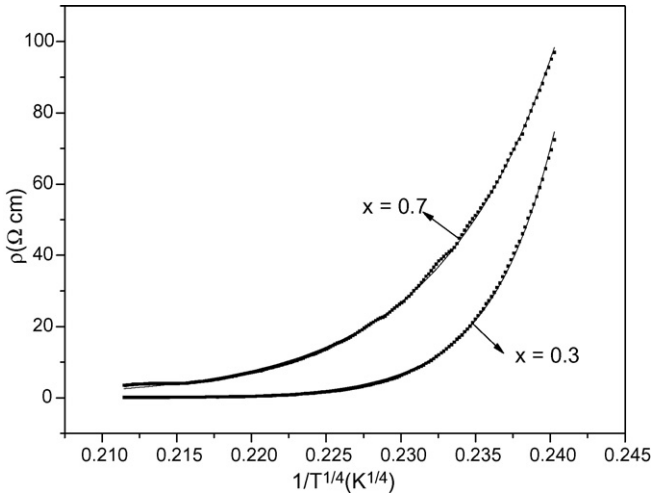

Fig. 8. Fitting curves for $x = 0.3$ and 0.7 samples based on $\rho = \rho_0 T_0/T)^{1/4}$ model.

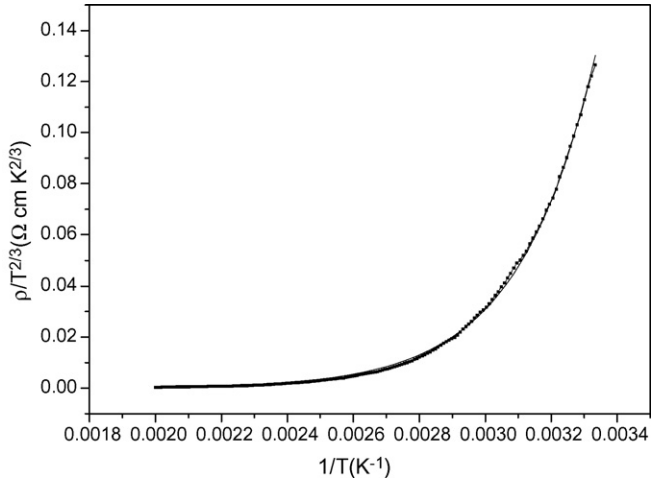

Fig. 9. Experimental data and calculating data based on $\rho = \rho_0 T^{3/2} \exp(E_A/kT)$ model.

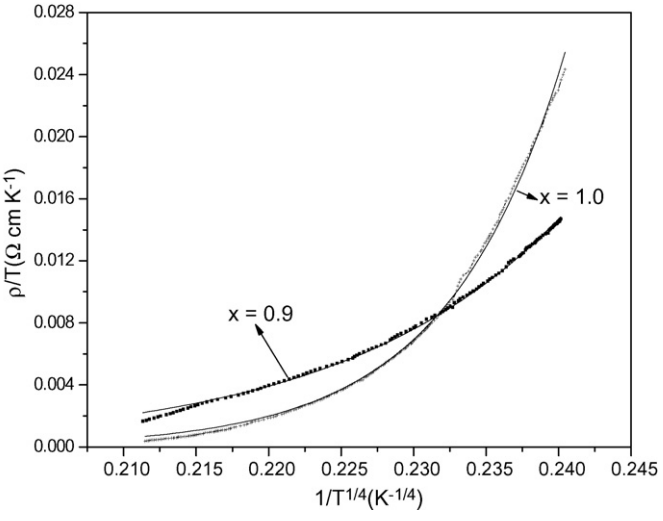

Fig. 10. Experimental data and fitting for $\rho = \rho_0 T \exp[E/kT + (T_0/T)^{1/4}]$ curves.

Table 3

$x = 0.1$ (E_A)	0.487 eV (H) 0.292 eV (L)
$x = 0.3$ (T_0)	2.99×10^9 K^{-1}
$x = 0.5$ (E_A)	0.314 eV
$x = 0.7$ (T_0)	2.57×10^8 K^{-1}
$x = 0.9$ (T_0)	1.78×10^7 K^{-1}
$x = 1.0$ (T_0)	2.41×10^8 K^{-1}

Fig. 7 demonstrates the electrical transport behavior for $x = 0.1$ sample at low temperature. It can be seen from Fig. 7 and the inset of Fig. 7 that adiabatic polaron model is confirmed at high temperature and bipolaron is identified at low temperature, respectively. For $x = 0.3$ and 0.7 specimens the electrical transport behaviors show in Fig. 8. One can be noticed that variable range hopping model is testified from $T = 300$ to 500 K. Fig. 9 presents the electrical transport behavior for $x = 0.5$ and it can be proved that the electrical transport mechanism is non-adiabatic polaron model. Fig. 10 demonstrates the electrical transport behaviors for $x = 0.9$ and 1.0 samples and two steps transport of small polarons model is confirmed. From the fitting curves the parameters of E_A and T_0 can be obtained and present in Table 3. From Table 3 one can be seen that these parameters are consistent with analysis of samples's resistivity.

4. Conclusions

The structure of series $Sm_{1-x}Ca_xFe_{1-x}Mn_xO_3$ ($0.0 \leq x \leq 1.0$) compounds were investigated. The lattice parameters increase with coupled substitution Sm^{3+} by Ca^{2+} and Fe^{3+} by Mn^{4+}. The variation of parameter, c, is larger than that of a and b, respectivly. The variation of cell parameter, a, is faster than that of b in the range from $0.0 \leq x \leq 0.5$ and change of lattice parameter, a, is slower than that of b in the range from $0.5 \leq x \leq 1.0$, indicating that the replacement of Sm^{3+} and Fe^{3+} by Ca^{2+} and Mn^{4+} is order. The detailed analysis of magnetic properties of series $Sm_{1-x}Ca_xFe_{1-x}Mn_xO_3$ ($0.1 \leq x \leq 0.9$) shows that local magnetic interaction between Fe^{3+}/Mn^{4+} and Fe^{3+}/Mn^{4+} at below magnetic transition temperature is antiferromagnetic. Above magnetic transition temperature the presence of large magnetic cluster is proposed and the sizes of magnetic clusters decrease with Mn^{4+} and Ca^{2+} content. The Curie–Weiss temperature seems to correlate with tolerance factor. The electrical behaviors of all specimens demonstrate insulator and the electrical resistivity decreases with Mn and Ca ionic doped. The detailing analysis of electrical transport shows that the electrical process of sample for $x = 0.1$ is controlled by adiabatic small polaron hopping model at high temperature and by bipolaron model at low temperature and that the electrical process of samples for $x = 0.3$ and 0.7 are dominated by variable range hopping and that electrical mechanism of sample for $x = 0.5$ is consistent with non-adiabatic small polaron hopping model and that the electrical behaviors of spencimens for $x = 0.9$ and 1.0 are agreed with two steps transport of small polaron model.

Acknowledgement

This work was supported by Foundation for Doctor, Education Department of Hebei Province (B2002102), PR China.

References

[1] K. Chahara, T. Ohno, M. Kasai, Y. Kozono, Magnetoresistance in magnetic manganese oxide with intrinsic antiferromagnetic spin structure, Appl. Phys. Lett. 63 (1993) 1990–1992.
[2] S. Jin, H.M. O'Bryan, T.H. Tiefel, M. McCormack, W.W. Rhodes, Large magnetoresistance in polycrystalline La–Y–Ca–Mn–O, Appl. Phys. Lett. 66 (1995) 382–384.
[3] R. Mahesh, R. Mahendiran, A.K. Raychaudhuri, C.N.R. Rao, Giant magnetoresistance in bulk samples of $La_{1-x}A_xMnO_3$ (A = Sr or Ca), J. Solid State Chem. 114 (1995) 297–299.
[4] A. Maignan, Ch. Simon, V. Caignaert, B. Hervieu, Giant magnetoresistance ratios superior to 10^{11} in manganese perovskites, Solid State Commun. 96 (1995) 623–625.
[5] H. Yoshizawa, H. Kawano, Y. Tomioka, Y. Tokura, Magnetic-field-induced metal-insulator transition in $Pr_{0.7}Ca_{0.3}MnO_3$, J. Phys. Soc. Jpn. 65 (1996) 1043–1052.
[6] H.Y. Hwang, S.W. Cheong, P.G. Radaelli, M. Marezio, B. Battlog, Lattice effects on the magnetoresistance in doped $LaMnO_3$, Phys. Rev. Lett. 75 (1995) 914–917.
[7] L.M. Rodriguez-Martinez, J.P. Attfield, Cation disorder and size effects in magnetoresistive manganese oxide perovskites, Phys. Rev. B 54 (1996) R15622–R15625.
[8] R. Ganguly, M. Hervieu, C. Martin, B. Raveau, Doping at the Mn site of the electron-doped manganite $Ca_{0.9}Ce_{0.1}MnO_3$, J. Phys.: Condens. Matter. 14 (2002) 9039–9052.
[9] A. Sundaresan, J.L. Tholence, A. Maignan, C. Martin, M. Hervieu, B. Raveau, E. Suard, Jahn-Teller distortion and magnetoresistance in electron doped $Sr_{1-x}Ce_xMnO_3$ ($x = 0.1, 0.2, 0.3$ and 0.4), Eur. Phys. J. B 14 (2000) 431–438.
[10] M. Auslender, A.I. Shames, E. Rozenberg, G. Gorodetsky, C. Martin, A. Maignan, Model of ground state in electron-doped $Ca_{1-x}Sm_xMnO_3$ ($0 < x \leq 0.20$) manganites and ferromanetic resonance probing of ''spontaneous ferromagnetism'' in $Ca_{0.8}Sm_{0.2}MnO_3$, J. Appl. Phys. 93 (2003) 8077–8079.
[11] H. Chiba, M. Kikuchi, K. Kusaba, Y. Muraoka, Y. Syono, Ferromagnetism and large negative magnetoresistance in $Bi_{1-x}Ca_xMnO_3$ ($x \geq 0.8$) perovskite, Solid State Commun. 99 (1996) 499–502.
[12] I.O. Troyanchuk, N.V. Samsonenko, H. Szymczak, A. Nabialek, Magnetic study of the $Ca_{1-x}Eu_xMnO_3$ ($0 \leq x \leq 1$) perovskites, J. Solid State Chem. 131 (1997) 144–149.
[13] C. Martin, A. Maignan, F. Damay, M. Hervieu, B. Raveau, CMR effect in electron-doped manganites $Ca_{1-x}Sm_xMnO_3$, J. Solid State Chem. 134 (1997) 198–202.
[14] A. Maignan, C. Martin, F. Damay, B. Raveau, Factor governing the magnetoresistance properties of the electron-doped manganites $Ca_{1-x}A_xMnO_3$ (A = Ln, Th), Chem. Mater. 10 (1998) 950–954.
[15] J. Takeuchi, A. Uemura, K. Miyoshi, K. Fujiwara, Colossal magnetoresistance and spin-glass behavior of the perovskite $Nd_{0.67}Sr_{0.33}Mn_{1-x}Fe_xO_3$, Physica B 281–282 (2000) 489–490.
[16] A. Simopoulos, M. Pissas, G. Kallias, E. Devlin, N. Moutis, I. Panagiotopoulos, D. Niarchos, C. Christides, Study of Fe-doped $La_{1-x}Ca_xMnO_3$ ($x \approx 1/3$) using Mossbauer spectroscopy and neutron diffraction, Phys. Rev. B 59 (1999) 1263–1271.
[17] L.K. Leung, A.H. Morrish, B.J. Evans, Magnetic properties of iron-doped manganites, Phys. Rev. B 13 (1976) 4069–4078.
[18] J.J. Blanco, M. Insausti, I. Muro, L. Lezama, T. Rojo, Neutron diffraction and magnetic study of the $Nd_{0.7}Pb_{0.3}Mn_{1-x}Fe_xO_3$ ($0 \leq x \leq 0.1$), J. Solid State Chem. 179 (2006) 623–631.
[19] S. Asthana, A.K. Nigam, D. Bahadur, Effect of cobalt substitution on magneto-transport properties of $Nd_{0.7}S_{r0.3}Mn_{1-x}Co_xO_3$ ($0.0 \leq x \leq 1$), J. Appl. Phys. 97 (2005) 1–3, 10C101.
[20] R.H. Mitchill, A.R. Chakhmouradian, A new series of complex perovskites $La_{1-x}Sr_xC_{r1-x}Ti_xO_3$: structural characterization, J. Solid State Chem. 144 (1999) 81–85.
[21] A.M. Glazer, The classification of titled octahedra in perovskites, Acta Crystallogr. Sect. B 28 (1972) 3384–3392.
[22] P.M. Woodward, T. Vogt, D.E. Cox, A. Arulraj, C.N.R. Rao, P. Karen, A.K. Cheetham, Influence of cation size on the structural features of $Ln_{1/2}A_{1/2}MnO_3$ perovskites at room temperature, Chem. Mater. 10 (1998) 3652–3665.
[23] F.F. Hanna, Structural study of $[Nd_{0.5}(Ca_{0.25}Ba_{0.25})MnO_3]$ and $[Nd_{0.5}(Ca_{0.25}Sr_{0.25})MnO_3]$ perovskites at room temperature, Egypt J. Sol. 24 (2001) 33–40.
[24] K.H. Ahn, X.W. Wu, K. Liu, C.L. Chien, Magnetic properties and colossal magnetoresistance of $La(Ca)MnO_3$ materials doped with Fe, Phys. Rev. B 54 (1996) 15299–15302.
[25] R.C. Budhani, C. Roy, L.H. Lewis, Q. Li, A.R. Moodenbaugh, Magnetic ordering and granularity effects in $La_{1-x}Ba_xMnO_3$, J. Appl. Phys. 876 (1999) 2490–3249.
[26] P.S.A. Kumar, P.A. Joy, S.K. Date, Evdence for Jahn–Teller polaron formation and spin-cluster-assisted variable-range-hopping conduction in $La_{0.7}Ca_{0.3}MnO_3$, J. Phys.: Condens. Matter. 10 (1998) L269–L275.
[27] J.Z. Sun, L. Krusin-Elbaum, A. Gupta, G. Xiao, S.S.P. Parkin, Does magnetization in thin-film manganates suggest the existence of magnetic clusters? Appl. Phys. Lett. 69 (1996) 1002–1004.
[28] J.M.D. Teresa, M.R. Ibarra, P.A. Algarable, C. Ritter, C. Marquina, J. Blasco, J. Garcia, A. Delmora, Z. Arnold, Evidence for magnetic polarons in the magnetoresistive perovskites, Nature (London) 386 (1997) 256–259.
[29] G.H. Joonker, Semiconducting properties of mixed crystals with perovskite structure, Physica 20 (1954) 1118–1122.
[30] E. Banks, N. Tashima, Magnetically ordered perovskites in the system $La_{1-x}Ca_xFe_{1-x}Mn_xO_3$, J. Appl. Phys. 41 (1970) 1186–1187.
[31] Y. Sun, X. Xu, Y. Zhang, Variable-range hopping of small polarons in mix-valence manganites, J. Phys.: Condens. Matter. 12 (2000) 10475–10480.